© 2018. Published by The Company of Biologists Ltd | Journal of Cell Science (2018) 131, jcs214346. doi:10.1242/jcs.214346

TOOLS AND RESOURCES

SunRiSE – measuring translation elongation at single-cell resolution by means of flow cytometry

Rafael J. Argüello[1,*,‡], Marisa Reverendo[1,*], Andreia Mendes[1], Voahirana Camosseto[1], Adrian G. Torres[3], Lluis Ribas de Pouplana[3,4], Serge A. van de Pavert[1], Evelina Gatti[1,2,*] and Philippe Pierre[1,2,*,‡]

ABSTRACT

The rate at which ribosomes translate mRNAs regulates protein expression by controlling co-translational protein folding and mRNA stability. Many factors regulate translation elongation, including tRNA levels, codon usage and phosphorylation of eukaryotic elongation factor 2 (eEF2). Current methods to measure translation elongation lack single-cell resolution, require expression of multiple transgenes and have never been successfully applied *ex vivo*. Here, we show, by using a combination of puromycilation detection and flow cytometry (a method we call 'SunRiSE'), that translation elongation can be measured accurately in primary cells in pure or heterogenous populations isolated from blood or tissues. This method allows for the simultaneous monitoring of multiple parameters, such as mTOR or S6K1/2 signaling activity, the cell cycle stage and phosphorylation of translation factors in single cells, without elaborated, costly and lengthy purification procedures. We took advantage of SunRiSE to demonstrate that, in mouse embryonic fibroblasts, eEF2 phosphorylation by eEF2 kinase (eEF2K) mostly affects translation engagement, but has a surprisingly small effect on elongation, except after proteotoxic stress induction.

This article has an associated First Person interview with the first author of the paper.

KEY WORDS: Puromycin, Translation elongation factor, B cell, T cell, Fetal liver, Protein synthesis

INTRODUCTION

Protein synthesis is a central metabolic process that is regulated at different biochemical levels. Polypeptide elongation by ribosomes proceeds discontinuously, with pauses regulating the speed of protein synthesis (Petersen et al., 2006; Richter and Coller, 2015). The total level of engaged ribosomes and the associated elongation rate are affected by translation elongation and initiation factors, codon usage, tRNA abundance and post-transcriptional modifications, as well as by different steric impediments, such as mRNA secondary structures or microRNA (miRNA) expression (Petersen et al., 2006; Richter and Coller, 2015). *In vitro* translation assays and ribosome profiling have recently demonstrated that elongation speed affects co-translational protein folding and protein expression (Buhr et al., 2016; Yu et al., 2015). The relative contribution of the different environmental and endogenous factors on translation elongation in cells directly isolated from human blood or mice tissues is poorly understood and is still methodologically demanding. Approaching these questions requires a technique with high-throughput potential and that measures translation elongation rates under physiological conditions in non-abundant and non-transformed cells *ex vivo*. Reduced manipulation and applicability to complex mixes of cells should also be a requirement for such a method. Among the techniques available for assessing translation elongation rates, one can distinguish methods that measure an average rate within a bulk of cells (Arava et al., 2003; Brar and Weissman, 2015; Dieterich et al., 2010; Ingolia et al., 2009; Starck et al., 2004) from those that measure translation rates at the single-mRNA molecule scale and require multiple steps of molecular engineering (Halstead et al., 2015; tom Dieck et al., 2015; Wang et al., 2016; Yan et al., 2016). The first group of methods includes ribosome profiling, polysome profiling and radiolabeled methionine incorporation assays. Given the advantages and recent improvements in next-generation sequencing, ribosome profiling has become a gold standard to monitor translation and ribosome engagement (McGlincy and Ingolia, 2017). This technique allows for qualitative and quantitative measurement of translation by sequencing RNA fragments that are 28 and 29 nucleotides long and are protected from degradation through their association with ribosomes. Single-cell ribosome profiling has, however, never been performed, and seems for the moment to be out of technical reach, leaving ribosome profiling approaches with the disadvantage of measuring translation through the averaging of many cells, sometimes from very heterogeneous populations, during which individual phenotypes are binned and diluted into one unique dataset.

Puromycin (puro) is an aminonucleoside Tyr-tRNA mimetic antibiotic that enters the A site of ribosomes, and is incorporated into nascent chains. Puro incorporation induces the termination of peptide synthesis, and this covalent reaction between nascent proteins and puro is called puromycilation (Azzam and Algranati, 1973). Puromycilation detection with ad hoc antibodies and measurement by flow cytometry has proven to be an extremely versatile method to replace radiolabeled amino acid incorporation as a means to monitor protein synthesis levels (Goodman et al., 2012; Schmidt et al., 2009). Here, we propose to combine puro immuno-detection together with 'run-off' experiments on translating ribosomes to determine the translation elongation rate in different cell populations, including human blood cells and mouse embryonic cells. Importantly, accurate rate measurements allow the direct comparison of protein synthesis activity in different cells types and tissues, independently of the variations observed in cell size, amount of ribosomes or environmental

[1]Centre d'Immunologie de Marseille-Luminy, Aix Marseille Université, Inserm, CNRS, 13288, Marseille Cedex 9, France. [2]Institute for Research in Biomedicine (iBiMED) and Ilidio Pinho Foundation, Department of Medical Sciences, University of Aveiro, 3810-193 Aveiro, Portugal. [3]Institute for Research in Biomedicine (IRB Barcelona), The Barcelona Institute of Science and Technology, Parc Científic de Barcelona, C/Baldiri Reixac 10, 08028 Barcelona, Catalonia, Spain. [4]Catalan Institute for Research and Advanced Studies (ICREA), P/Lluis Companys 23, 08010 Barcelona, Catalonia, Spain.
*These authors contributed equally to this work

‡Authors for correspondence (arguello@ciml.univ-mrs.fr; pierre@ciml.univ-mrs.fr)

M.R., 0000-0001-6999-1816; V.C., 0000-0003-1167-6279; A.G.T., 0000-0002-5479-1325; L.R., 0000-0002-2087-0359; S.A.v., 0000-0002-7147-4380; E.G., 0000-0002-0667-0799; P.P., 0000-0003-0863-8255

Received 13 December 2017; Accepted 4 April 2018

Journal of Cell Science (2018) 131, jcs214346. doi:10.1242/jcs.214346

growth conditions. This novel method called 'SunRiSE' (for SUnSET-based Ribosome Speed of Elongation; SUnSET refers to 'Surface sensing of translation') offers novel exploratory capabilities, which are illustrated here by an analysis of protein synthesis in normal and stress conditions after genetic inactivation of translation elongation factor 2 kinase (eEF2K) in mouse embryonic fibroblasts (MEFs). Surprisingly, eEF2K ablation mostly affects ribosome engagement, and most likely protein synthesis initiation at steady state, rather than ribosome processing speed. The impact of eEF2K on translation elongation is, however, revealed upon ER-stress induction, since the translation intensity and elongation rate in eEF2K-deficient cells remain unaffected by tunicamycin treatment. Interestingly, the levels of phosphorylated eEF2 (P-eEF2) are highly heterogeneous among single wild-type (WT) MEFs grown in the same culture conditions, and SunRiSE reveals that eEF2 phosphorylation at steady state does not necessarily correlate with a lower protein synthesis rate. The existence of such biochemical heterogeneity further demonstrates the importance of developing novel techniques, like SunRiSE, to measure protein synthesis at high resolution and study its impact on the control of protein expression.

RESULTS

A combination of puro labeling and ribosome run-off to measure the translation elongation rate

By using puro as a nascent protein tag and anti-puro monoclonal antibodies for its detection, we have previously introduced puro-immunomonitoring and, in particular, flow cytometry to measure translation in living cells and organisms (Schmidt et al., 2009; Seedhom et al., 2016). Surface sensing of translation (SUnSET) allows for measuring global translation in individual cells found in mixed populations grown *in vitro* or *ex vivo*. Despite these clear advantages, quantitative SUnSET measurements are not absolute and can only be performed relative to a given reference sample, and are therefore not adapted for a direct comparison among many cellular samples of different origins and obtained at different times. A precise measure of a translation elongation rate in different populations should, however, solve this issue, by attributing an elongation rate constant to each specific cell group. Such a rate constant would allow a direct quantitative comparison of variations in protein synthesis activity among different cells present in heterogeneous populations or tissues, and growing in different environmental conditions.

In addition to puro, antibiotics interfering with ribosome assembly and function have proven to be invaluable reagents to study translation mechanisms, and in particular initiation and elongation. Harringtonine efficiently blocks the initiation of elongation during protein synthesis, and thus had been used with ribosome profiling in run-off experiments to establish the rate of elongation of mammalian ribosomes (~330 codons/min) (Ingolia et al., 2012). We hypothesized that the rate of translation elongation in single cells could be established by measuring puro incorporation by flow cytometry after blocking translation initiation with harringtonine at different time intervals (Fig. 1). The decay in

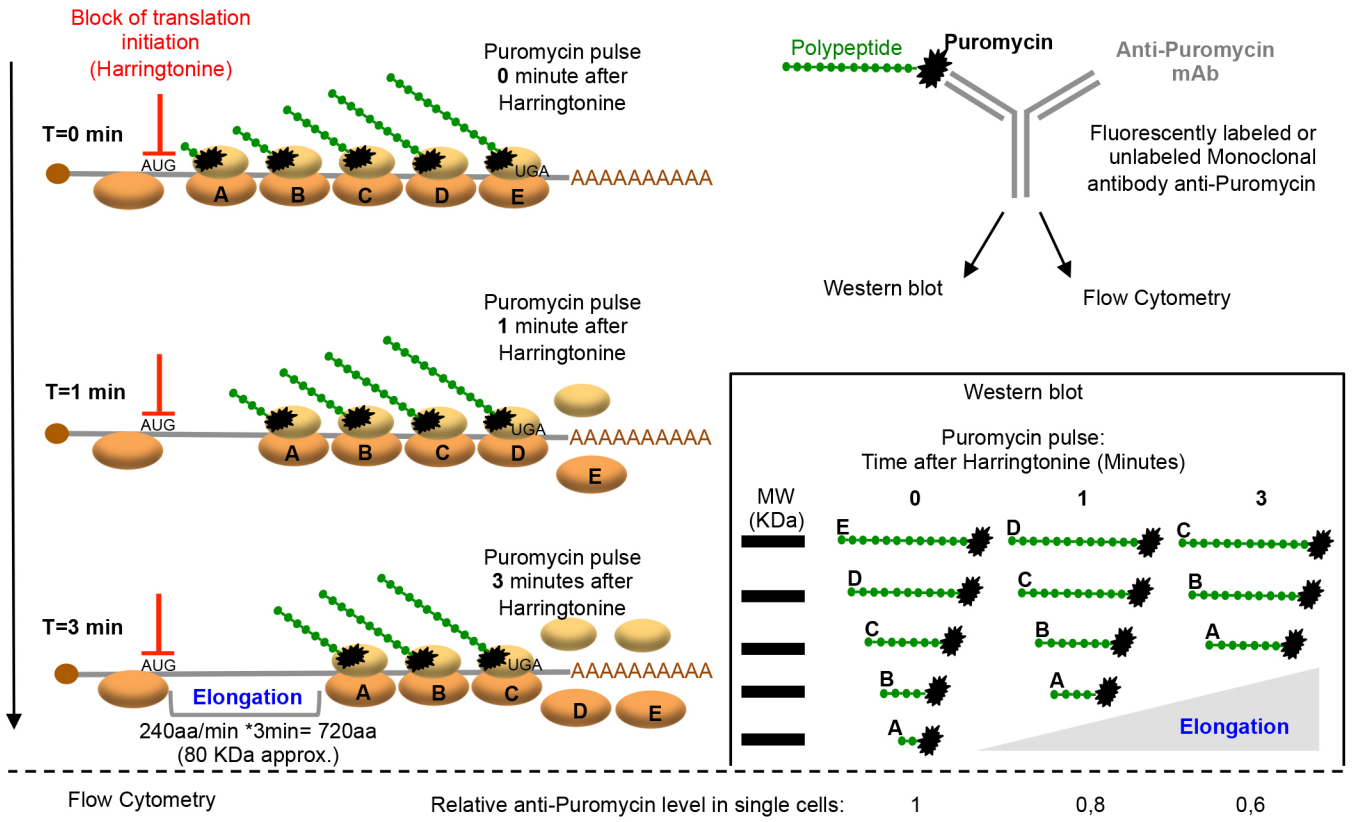

Fig. 1. Schematic representation of the SunRiSE protocol and results. Cells are seeded in culture wells, and translation initiation is blocked by addition of harringtonine at time 0. Puro is added at different times after inhibition of translation initiation and is incorporated into nascent peptides by elongating ribosomes (denoted A–E). After a certain time of harringtonine treatment, pre-engaged ribosomes continue to elongate, and thus ribosomes that were bearing short peptides at T0, are associated with longer peptides after 240 s of treatment. Eventually translating ribosomes run-off from mRNAs, and the gap between the last initiating ribosomes and the translation initiation site will directly correlate with the elongation rate of the ribosomes, and therefore inversely correlate to the amount of puro incorporation. Puro incorporation is revealed by immunodetection through immunoblotting and flow cytometry, allowing a measure of puro incorporation decay (which correlated to the translation elongation rate) in bulk or at single-cell resolution. MW, molecular mass; aa, amino acids.

Journal of Cell Science

Journal of Cell Science (2018) 131, jcs214346. doi:10.1242/jcs.214346

puro labeling upon harringtonine treatment is linked to the speed at which ribosomes run-off from mRNAs, and therefore directly provides an accurate measure of the global translation elongation rate (Fig. 1). We first established the kinetics at which polysomes are lost upon harringtonine treatment by following the rRNA distribution after sucrose gradient separation. Most polysomes were found to run-off from mRNAs within 8 min of translation initiation inhibition (Fig. 2A), and remained completely stabilized after treatment with the nascent chain elongation inhibitor emetine (David et al., 2013). Upon addition of puro at various times (30 s to 1 min) after harringtonine treatment, a decay in the incorporation of the nucleosidic antibiotic into neosynthetized proteins was observed by immunoblotting (Fig. 2B). Again, the loss of puro labeling upon translation initiation arrest was prevented by blocking translation elongation with emetine. As a consequence of ribosome elongation during translation initiation inhibition, loss of puro labeling was first observed within the population of small nascent proteins and, later on, in larger peptides displaying higher molecular masses (Fig. 2B,C). Taken together, these results indicate that puro incorporation decay after inhibition of the first round of translation elongation, provides an accurate measure of the processing speed of ribosomes along mRNAs, thus supporting our initial hypothesis, and calling us to explore the large potential of this method, termed 'SUnSET-based Ribosome Speed of Elongation' (SunRiSE), by switching to flow cytometry monitoring of puromycin incorporation.

Multiparametric monitoring of translation elongation rate by flow cytometry

We optimized SunRiSE for flow cytometry by adjusting the puro concentration, and using 12D10 anti-puro antibody conjugated directly to Alexa® Fluor (AF) dyes (e.g. AF488 and AF647). The puro incorporation decay in presence of harringtonine was first measured in HeLa cells (Fig. 3A), and graphically plotted as

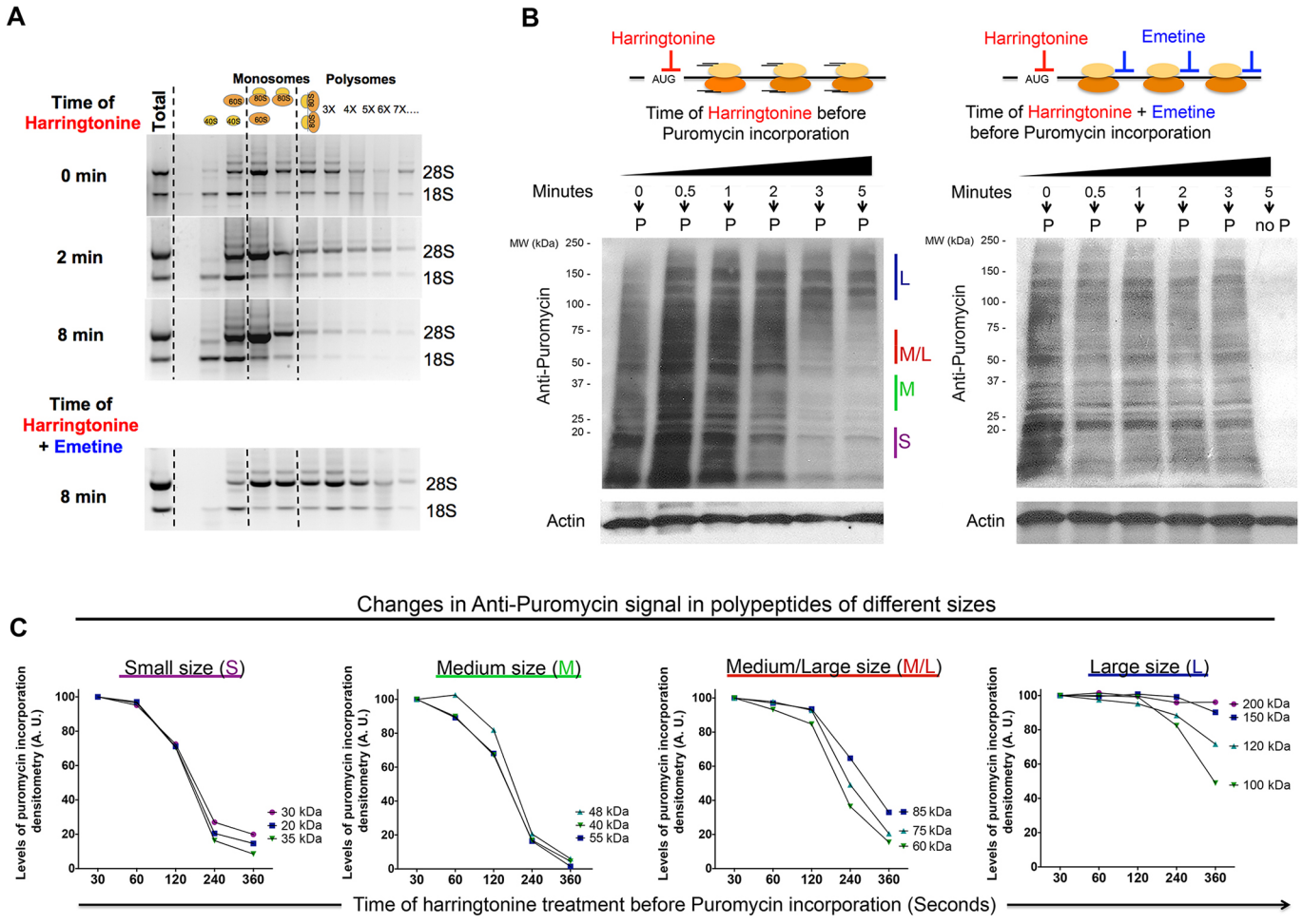

Fig. 2. Visualization and validation of translation elongation by polysome isolation and SunRiSE. (A) WT MEFs treated with 2 µg/ml of harringtonine for the indicated times were lysed and subjected to ultracentrifugation on a sucrose density gradient (upper panel, 0, 2 and 8 min). Gradient fractions were collected and rRNA was extracted and separated by agarose electrophoresis. In order to compare changes in polysome separation profiles, the same procedure was applied to MEFs treated with harringtonine and the translation elongation inhibitor emetine (Fig. 2A, lower panel). Representative results from *n*=3 experiments are shown. Non-fractionated total RNA was extracted and loaded in lane 1 as a control. (B) WT MEFs treated with 2 µg/ml of harringtonine for the indicated times (0, 0.5, 1, 2, 3 and 5 min) and subsequently treated with puro (10 µg/ml) for 10 min. Cells were lysed and subjected to immunoblotting with anti-puro antibody (left). Emetine was included in control samples to measure the stability of puro incorporation in absence of translation elongation. (C) Quantification and graphical representation of puro incorporation over time in relationship to the different nascent protein sizes observed in B (left). As expected, inhibition by means of harringtonine initially prevents the incorporation of puro in short polypeptides, and later in larger molecular mass polypeptides requiring longer time for their synthesis. Representative results from *n*=3 experiments. A.U. arbitrary units.

Journal of Cell Science

Journal of Cell Science (2018) 131, jcs214346. doi:10.1242/jcs.214346

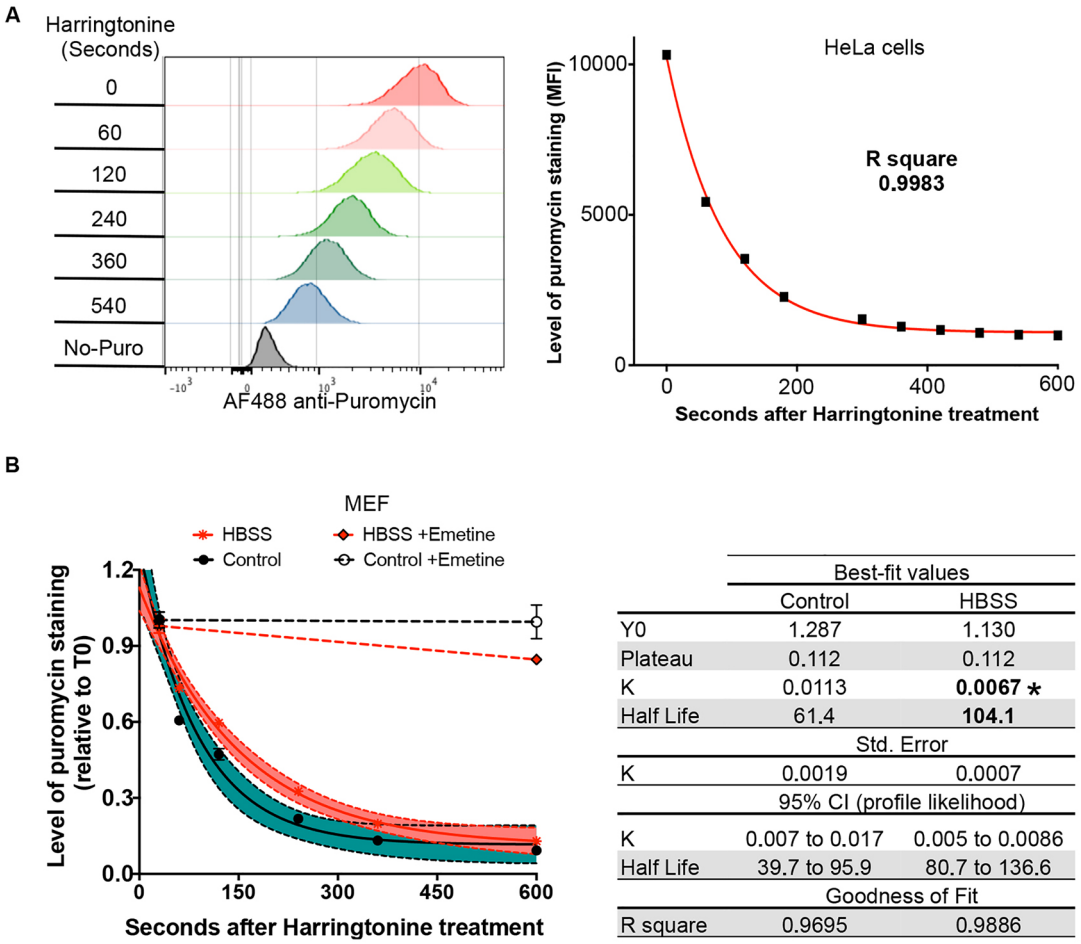

	Best-fit values	
	Control	HBSS
Y0	1.287	1.130
Plateau	0.112	0.112
K	0.0113	**0.0067 ***
Half Life	61.4	**104.1**
	Std. Error	
K	0.0019	0.0007
	95% CI (profile likelihood)	
K	0.007 to 0.017	0.005 to 0.0086
Half Life	39.7 to 95.9	80.7 to 136.6
	Goodness of Fit	
R square	0.9695	0.9886

Fig. 3. SunRiSE application using flow cytometry for multiple parameters analysis in single cells. (A) HeLa cells were treated with harringtonine (2 µg/ml) for different times (harringtonine, seconds) prior to incubation with puro (10 µg/ml) and detection with Alexa Fluor 488 (AF488)-conjugated anti-puro antibody by means of flow cytometry. Histograms of different colors show the distribution of fluorescence labeling intensity measured in 30,000 cells for each time point. The mean fluorescence intensity (MFI, black squares) of the whole population was obtained from the histograms (left) and is plotted as a function of time (right). The decrease in puro incorporation over time fits a single-phase logarithmic decay curve (in red, non-linear regression, r=0.9983). (B) SunRiSE was applied to MEFs to monitor the rate of translation elongation during starvation. 80% confluent MEFs were incubated in HBSS without serum for 4 h, prior to harringtonine and puro treatment, fixation, permeabilization, and staining with AF488-conjugated anti-puro antibody. After flow cytometry, the mean±s.e.m. levels of puro MFI (six time points in duplicate) were normalized to those at t=0 (T0) and datasets subjected to non-linear regression using GraphPad Prism software (the 95% c.i. is shown in red and teal for HBSS-treated and control cells). The results are representative of three independent experiments. Statistical significance (*P<0.05) was assigned by PRISM software after comparing k values for the 95% c.i. in HBSS versus control cells. The best fit values for the non-linear regression (r^2>0.95) are shown in the table.

a one-phase logarithmic decay curve (R=0.998), described by the function:

$$puro_{(t)} = \frac{(puro_{\text{initial}} - puro_{\text{plateau}})}{e^{k \times t}} + puro_{\text{plateau}},$$

where the k value is a constant related to the elongation rate of the ribosomes in a given cell population.

When elongation is blocked by emetine, k tends towards zero, and anti-puro staining levels at different time points remain constant and equal to $puro_{\text{initial}}$ at all times points [$e^{0 \times t}$=1, then puro(t)=puro$_{\text{initial}}$]. k values therefore permit a direct comparison of elongation rates in situations during which many parameters fluctuate, and different intensities of protein synthesis are displayed by distinct cell groups. A comparative measurement of translation elongation rates upon HBSS starvation of mouse embryonic fibroblasts (MEFs) is shown in Fig. 3B to illustrate this point. It has been previously shown, through ribosome profiling, that a decrease in the elongation rate of polysomes can be observed in starving MEFs (Ingolia et al., 2012). We could confirm this observation by performing SunRiSE after 4 h of HBSS starvation and measuring k values, which were reduced by half compared to normally fed control cells (Fig. 3B).

We next performed multi-parametric analysis of single cells present in a complex suspension of spleen cells (Fig. 4). Mouse splenocytes were chosen as an experimental model, given their large heterogeneity, the availability of multiple cell-specific markers suitable for flow cytometry analysis, and their capacity to undergo rapid changes in protein synthesis intensity upon stimulation with bacterial lipopolysaccharides (LPS) (Lelouard et al., 2007) or a cocktail of phorbol 12-myristate 13-acetate (PMA) and ionomycin (Schmidt et al., 2009). Our experiments were designed to monitor the total levels of protein synthesis in different cell populations simultaneously, but more importantly, to define whether elongation

Journal of Cell Science (2018) 131, jcs214346. doi:10.1242/jcs.214346

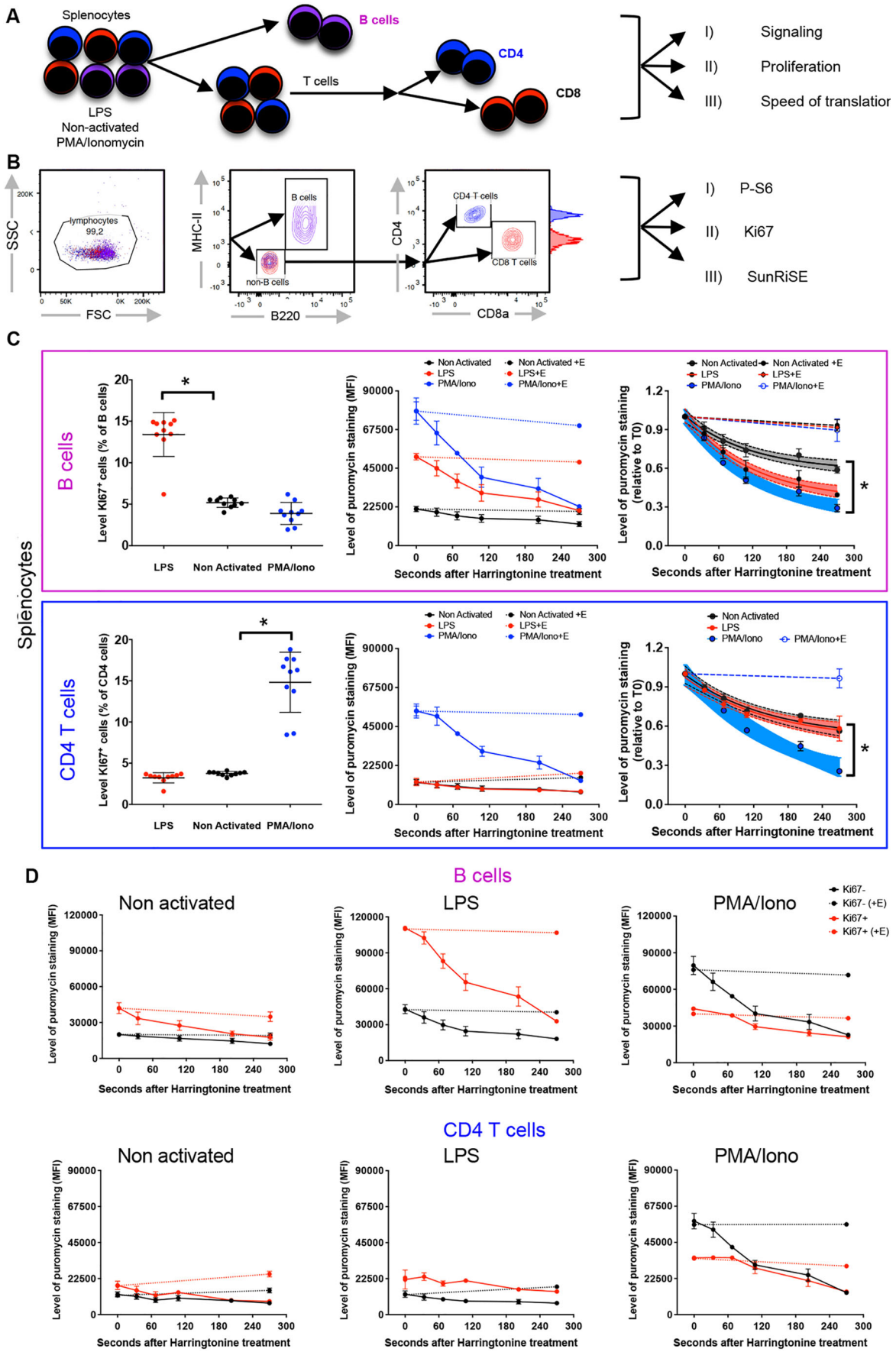

Fig. 4. See next page for legend.

Journal of Cell Science

Journal of Cell Science (2018) 131, jcs214346. doi:10.1242/jcs.214346

Fig. 4. Multiple parameters flow analysis of mouse splenocytes by SunRiSE. Mouse splenocytes were isolated and incubated for 16 h with 10 ng/ml of PMA and 1 ng/ml of ionomycin (PMA/Iono), or LPS (100 ng/ml) or were not stimulated (control). SunRiSE was performed together with CD4, CD8, CD19, CD11c, MHC-II and B220 flow cytometry staining to identify B and T Cells, as well as Ki67 and ribosomal P-S6 identification, to evaluate entry into the cell cycle and S6K1/2–mTORC1 activation. (A) Diagram summarizing the experiment. (B) Flow cytometry gating strategy used to analyze translation, cell cycle and the mTORC1 axis activation in each lymphocyte subset present in the splenocyte population. (C) Percentage of cells showing Ki67 expression (left) and mean fluorescence intensity (MFI, middle) of anti-puro staining in control, LPS- or PMA/ionomycin-activated B cells (top, magenta frame) and $CD4^+$ T cells (bottom, blue frame). The total anti-puro MFI (center) or the value normalized at t=0 (T0) are shown for both the B cell and $CD4^+$ T cell populations plotted as a function of time. The associated non-linear regression (single-phase logarithmic decay) fit curve is shown on the right. Emetine addition (depicted as +E) was used to inhibit translation elongation ($k \approx 0$, dashed lines) and serves as a control. (D) MFI of puro incorporation in control or activated B cells (top) and T $CD4^+$ cells (bottom), segregated as $Ki67^+$ or $Ki67^-$ populations and plotted as a function of time. For the percentage of Ki67-positive cells, the same treatment was performed in different mice (n=3) and statistical significance (*P<0.05) was assigned using a two-tailed t-test. In C, the mean±s.e.m. levels for the puro MFI (six timepoints in duplicate) are plotted, and datasets subjected to non-linear regression (the 95% c.i. are shown in gray, red and blue, for control, LPS and PMI/Iono-treated cells, respectively). The results are representative of one experiment (n=3, performed in duplicate). Statistical significance (*P<0.05) was assigned using PRISM software after comparing k values for the 95% c.i. in control versus LPS- or PMA/Iono-treated cells.

rates are modified in different lymphocytes subsets after activation or cell cycle initiation (Fig. 4A). Flow cytometry was performed, using a gating strategy in which B cells were identified as $CD4^-$ $CD8^-$ $CD11c^-$ $CD19^+$ $B220^+$ MHC-II^+ cells, and $CD4^+$ T cells by a $CD4^+$ $CD8^-$ $CD19^-$ $CD11c^-$ MHC-II^- $B220^-$ phenotype (Fig. 4B). Phosphorylation of the ribosomal protein S6 (P-S6) (Lelouard et al., 2007) and the active cell cycle marker Ki67 (also known as MKI67) (Yu et al., 1992) were used, respectively, to evaluate metabolic activation (e.g. AKT/mTOR signaling axis) and entry in cell cycle within 16 h of stimulation (Fig. 4B,C). In B cells, overnight stimulation with PMA increased both global translation levels and speed of elongation, but did not augment the proportion of $Ki67^+$ cells (Fig. 4C). In contrast, LPS treatment induced Ki67 expression and augmented the translation elongation rate. Both LPS and PMA/ionomycin treatment induced an increase in P-S6 levels in B cells, suggesting that translation upregulation is generally associated with S6 phosphorylation, but not necessarily with cell cycle entry. The translation rates (k) of cells stimulated with PMA were different from those triggered by LPS, demonstrating that SunRiSE is sensitive enough to discriminate among different levels of activation and translation regulation. As expected from previous work, showing that LPS does not affect T cell proliferation nor cytokine secretion (Zanin-Zhorov et al., 2007), $CD4^+$ T cells only responded to PMA/ionomycin by increasing cycling and S6 phosphorylation (Fig. S1), while augmenting both protein synthesis intensity and associated translation elongation rate (Fig. 4C).

During mitosis, the overall level of protein synthesis has been described to be 35% lower, with some specific mRNAs showing an up to 10-fold reduction in their translation rate (Tanenbaum et al., 2015). The cell cycle induction triggered by PMA/ionomycin in $CD4^+$ T cells gave us the opportunity to comparatively measure translation rates in proliferating cells based on Ki67 antigen positivity or carboxyfluorescein succinimidyl ester (CFSE) labeling over 2 days of activation (Fig. 4D; Fig. S2). This enabled us to determine the level of translation and elongation in cells that had undertaken a different number of divisions. PMA-stimulated $Ki67^-$ T cells displayed a higher translation intensity and elongation rate than their $Ki67^+$ counterparts, a situation also observed in the small fraction of PMA-activated B cells found to be $Ki67^+$ (Fig. 4D). However, contrasting with PMA/ionomycin activation, LPS-activated $Ki67^+$ B cells displayed a 4-fold higher translation intensity and elongation rate than non cycling cells (Fig. 4D).

These results also reflected the level of S6 phosphorylation found in the different populations, P-S6 being mostly associated with a low level of Ki67 in PMA-stimulated T cells but not in PMA-stimulated B cells (Fig. S1). CFSE dilution experiments revealed similar differences, with the largest number of divisions observed respectively in PMA/ionomycin-stimulated T cells and LPS-activated B cells (Fig. S2A,B).

When SunRiSE was performed together with CFSE labeling, we could also unravel major differences in protein synthesis activity within the pool of proliferating cells (Fig. S2C,D). Both control and LPS-stimulated T cells had similar puromycin incorporation profiles, with only a small cell population, characterized by a low level of CFSE dilution, that displayed measurable translation activity. Conversely, PMA/ionomycin treatment strongly increased translation initiation and elongation in most T cells, although proportionally to the level of CFSE dilution exhibited (Fig. S2C), thus giving more resolute information than achieved through Ki67 staining alone. Our results indicate that after 2 days of PMA/ionomycin stimulation, protein synthesis activity is augmented proportionally to the number of cycles achieved. In LPS-stimulated B cells, protein synthesis was strongly enhanced in all cells; this was independently of the CFSE dilution level achieved and in full agreement with the results obtained with Ki67 staining after overnight stimulation (Fig. 4). Although, PMA induced a much weaker response in B cells than in T cells, the same relationship between CFSE dilution and increased protein synthesis activity was observed (Fig. S1D). Thus, cycling and translation regulation are highly interdependent and their relationship is influenced differently by the nature and duration of the activation stimuli. Importantly, PMA/ionomycin impacts the level of translation proportionally to the number of divisions achieved by the stimulated cells, a situation different from that observed with LPS stimulation and not entirely reflected by Ki67 expression.

SunRISE reveals that different subsets of embryonic liver cells display variable translation intensity and elongation rate

At the cellular level, the embryonic development program is an extremely complex, and coordinated cell migration, proliferation and differentiation, displaying different needs for protein synthesis activity, is required in order for it to be successful. SunRiSE is therefore well suited to characterize such embryonic cells on the basis of their translational activity rather than uniquely on their phenotype. Embryonic day (E)12.5 mouse embryos were obtained and fetal livers were processed (van de Pavert and Vivier, 2016) to perform flow cytometry analysis using specific markers of blood vessel endothelial cells (BVECs; $CD45^-$, $CD31^+$), Lyve+ sinusoidal endothelial cells (LyVECs; $CD45^-$, $CD31^{intermediate}$, $LyVE1^+$), hematopoietic stem cells and leukocytes (CD45+), as well as putative neuronal cells (Neuro; $CD45^-$, $CD24^+$) (Fig. 5A). Large variations in levels of puro incorporation and elongation rates could be observed among the different gated cells populations (Fig. 5B,C), underlining the metabolic differences already in place at this stage of development. Vascular endothelial cells displayed the lowest intensity of protein synthesis, probably indicating their high level of differentiation (Fig. 5C). Conversely, the highest translation rates were found in $CD45^+$ cell

Journal of Cell Science (2018) 131, jcs214346. doi:10.1242/jcs.214346

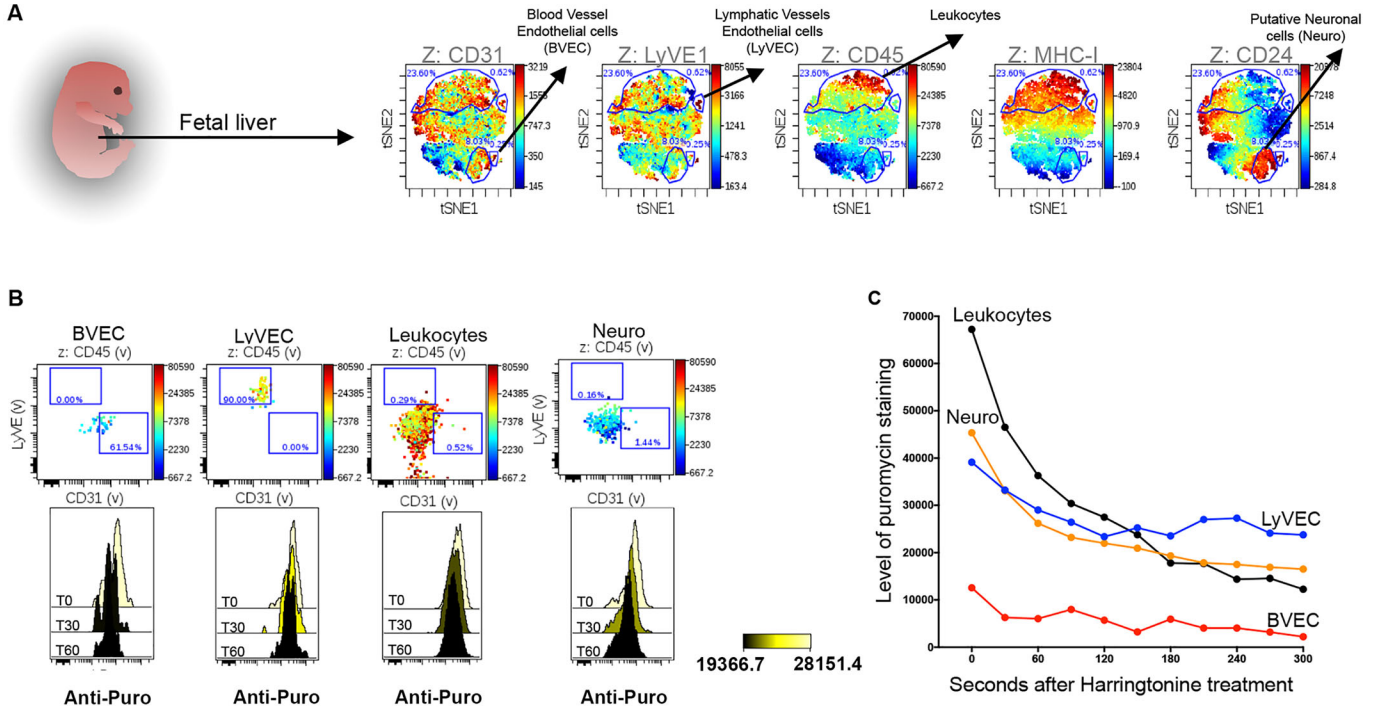

Fig. 5. Multiple parameters flow analysis of fetal liver cells by SunRiSE. (A) Single-cell suspensions of E12.5 fetal livers were submitted to SunRiSE. Cells were stained with a combination of antibodies (see Materials and Methods for more detail) against surface antigens and puromycin. The levels of CD31, LyVE1, CD45, MHC-I and CD24 expression were used to perform unsupervised clustering of the cells to determine cell subpopulations (t-SNE, Cytobank software). Different populations of cells, characterized by certain marker combinations, were observed at differing time points after harringtonine treatment (0, 30 and 60 s, denoted T0, T30 and T60). These cell populations include LyVECs (Lyve1$^+$), leukocytes (CD45$^+$), BVECs (CD31$^+$) and putative neuronal cells (Neuro, CD45$^-$ CD24$^+$). (B) Histogram overlay of the level of puro in each cell population at T0, T30 and T60. The heat map represents calculated raw values of medians in the anti-puromycin channel (*x*). (C) Graph including all time points and cells populations shown in A. Mean levels of puro MFI (11 time points) are plotted and datasets subjected to non-linear regression. The results are representative of different embryos analyzed (*n*=3, in duplicate).

populations with high differentiation potential (Fig. 5C). The relatively homogeneous rates of elongation among the different cell types (with the exception of the BVECs), suggests that translation initiation or engagement is likely to be a major post-transcriptional regulatory step used during lymphoid organ development, as has already been proposed for many other biological systems. Initiation appears, however, to be tightly coordinated with ribosome processing and translation elongation, suggesting the existence of common regulatory pathways coordinating these two key mechanistic aspects of protein synthesis. Large variations in translation activity are also likely to represent major differences in ATP production and amino acid availability in the different embryonic cells tested and could give important clues about cell fate and differentiation potential, in relation to their metabolic status.

Revisiting the importance of eEF2K in translation regulation

One of the major biochemical mechanisms that regulates translation elongation is the phosphorylation of elongation factor-2 (eEF2), the main, if not unique, substrate of eEF2K (Lazarus et al., 2017; Ryazanov, 2002). eEF2 phosphorylation is inhibitory and represses translation elongation in adverse growth conditions. Cellular stress, such as starvation, or accumulation of misfolded proteins in the endoplasmic reticulum, activate eEF2K, which in turn phosphorylates eEF2 and inhibits translation elongation through what is believed to be an arrest of codon translocation from ribosomal A to P sites (De Gassart and Martinon, 2017; Richter and Coller, 2015). SunRiSE is therefore an ideal technique to quantify, in different cells, the impact on translation elongation of eEF2K-mediated phosphorylation in normal or stressful growth conditions.

We first analyzed mouse embryonic fibroblasts (MEFs) isolated from *eEF2K*-deficient (−/−) or WT animals (Moore et al., 2015) for their capacity to phosphorylate eEF2 in normal conditions or upon tunicamycin-induced ER stress, and how this impacted on their translation elongation rates. Immunoblotting revealed the total absence of phosphorylated eEF2 (P-eEF2) in *eEF2K*$^{-/-}$ MEFs, and their incapacity to increase P-eEF2 upon tunicamycin treatment (Fig. 6A). Flow cytometry confirmed this result, but also demonstrated that, in steady state, P-eEF2 levels are extremely heterogeneous across individual fibroblasts (Fig. 6A), and that SunRiSE offers a mean for dissecting the role of P-eEF2 with single-cell resolution.

When protein synthesis and translation elongation rate were measured (Fig. 6B), *eEF2K*$^{-/-}$ MEFs displayed a clear increase in global translation activity compared to WT cells. In contrast, elongation speed was found to be identical among the two cell types, suggesting that permanent ablation of eEF2K increases translation engagement, rather than elongation speed per se. This was an unexpected result, given the reported activity of eEF2 *in vitro* (Herbert and Proud, 2006) and the presence of a low level of P-eEF2 at steady state in WT MEFs, which should have put a cap on elongation rate. When the same experiments were conducted with cells under persistent tunicamycin-induced ER-stress (16 h, Fig. 6C), we could observe that eEF2K deletion prevented both eEF2 phosphorylation and the downregulation of protein synthesis induced by tunicamycin. Both translation initiation and elongation activities were modestly impacted in *eEF2K*$^{-/-}$ cells, while they were considerably decreased in stressed WT cells. Thus, eEF2K and P-eEF2 control ribosome engagement, potentially through interference with translation initiation or early elongation events.

Journal of Cell Science (2018) 131, jcs214346. doi:10.1242/jcs.214346

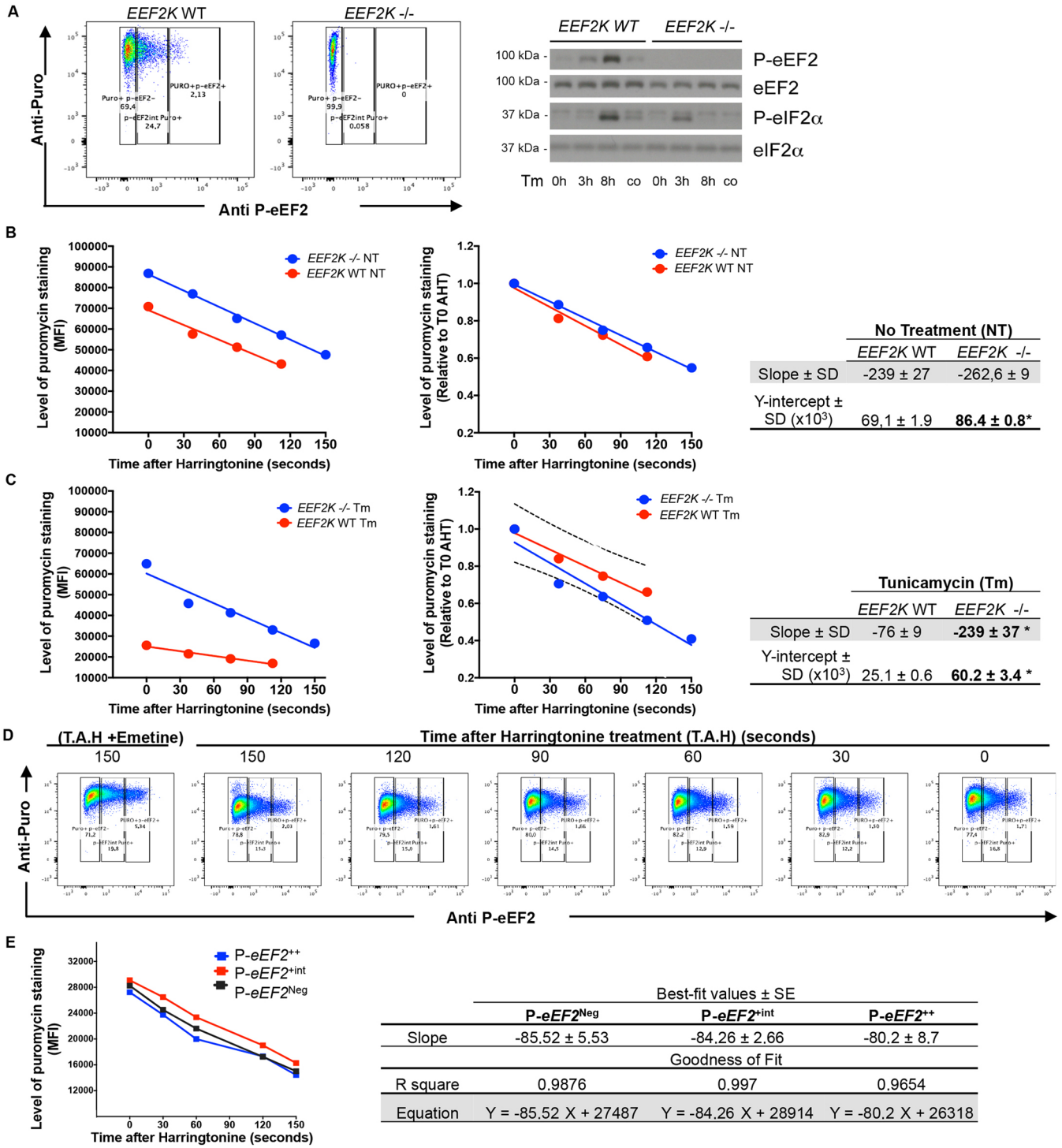

Fig. 6. SunRiSE applied to WT or *eEF2K*$^{-/-}$ MEFs. (A) WT and *eEF2K*$^{-/-}$ MEFs under normal growth conditions were incubated with rabbit anti-P-eEF2 antibodies, followed by AF647-conjugated mouse anti-rabbit-IgG and AF488-conjugated mouse anti-puromycin and analyzed by FACS (left). Levels of P-eEF2 as determined by immunoblotting in WT and *eEF2K*$^{-/-}$ MEFs measured through staining in cells under normal growth conditions or in cells treated overnight with the ER stressor tunicamycin (Tm). (B) Absolute (left) or relative (right) levels of anti-puro MFI staining as a function of time after harringtonine treatment in WT and *eEF2K*$^{-/-}$ in the absence of treatment (NT) or presence (C) tunicamycin (Tm). Bold asterisks in the table indicate statistically significant differences (P<0.05) between WT and *eEF2K*$^{-/-}$. (D) Flow cytometry dot plots depicting the subsets of WT MEFs with different levels of P-eEF2 under normal growth conditions. (E) The decrease in the level of puro in WT MEFs, at different times (1 to 150 s) after harringtonine is observed in all subsets and is plotted as a function of time. Best fit values±s.e.m. of the linear regression (r>0.95) are shown in the table. Statistically significant differences were not found (P>0.05). Results are representative of three independent experiments.

Alternatively, eEF2K ablation could increase global mRNA transcription and/or stabilization by decreasing the amount of ribosome run-offs from mRNA. The levels of eIF2α phosphorylation were increased in both cell types, however, to a lower level and with faster kinetics in *eEF2K*$^{-/-}$ MEFs (Fig. 6A), suggesting a strong interplay among the eEF2K and PERK (also

Journal of Cell Science (2018) 131, jcs214346. doi:10.1242/jcs.214346

known as eIF2AK3) pathways. Decreased eIF2α phosphorylation could therefore contribute to the resistance of *eEF2K*$^{-/-}$ MEFs to tunicamycin-induced translation arrest. With this in mind, we tested the respective contribution of eIF2α and eEF2 phosphorylation by using the pharmacological ISR inhibitor (ISRIB), which prevents inhibition of eIF2B and promotes translation initiation and stress granule assembly despite eIF2α phosphorylation (Sekine et al., 2015; Sidrauski et al., 2015). As expected, WT MEFs showed a rapid decrease in their translation activity upon a short treatment with thapsigargin, which was fully rescued in the presence of ISRIB (Fig. S3). In contrast, *eEF2K*$^{-/-}$ MEFs again displayed a modest inhibition of protein synthesis during acute ER stress, which was partially rescued by ISRIB. These results further confirm that the moderate inhibition of translation observed in *eEF2K*$^{-/-}$ MEFs is associated with reduced levels of eIF2α phosphorylation. eEF2K activity is therefore absolutely necessary to arrest ribosomal engagement upon ER stress, potentially through a strong interplay with the eIF2α phosphorylation pathway.

We next sought to investigate the consequences of the natural variations observed in P-eEF2 levels at the single-cell level. The differences in eEF2 phosphorylation were clearly dependent on eEF2K activity (Fig. 6A,D) and would have remained undetected by traditional bulk analysis, such as ribosome profiling. During SunRiSE analysis of WT MEFs, three subsets of cells were identified by the heterogeneous display of low, intermediate and high P-eEF2 levels (Fig. 6D,E), although eEF2 levels were found to be extremely homogeneous across the entire population (Fig. S4). To our surprise, and despite the high levels of P-eEF2 found in at least one of the subsets, no differences were observed in protein synthesis intensity nor in elongation rates among the different identified MEF subsets (Fig. 6E). These results suggest that in cell culture conditions, single cells display different eEF2K activity and P-eEF2 levels, but they demonstrate a great tolerance to these variations, probably by setting up adapted molecular thresholds of activation by stress. These stochastic thresholds allow each individual cell to commensurate its protective response by matching the inhibition of translation initiation (lower levels of phosphorylation) and translation elongation (higher levels of phosphorylation) to the intensity and duration of stress exposure.

DISCUSSION

Protein synthesis is one major regulatory layer that controls the final protein expression level. The translation machinery can rapidly react to environmental and metabolic cues and fine-tune the protein production issued from a pre-existing pool of mRNAs prior to major transcription reprogramming. Although mechanistic deciphering of the translation reaction was initiated in the 1950s, quantitative, or even qualitative, measurement of its efficacy in cells and tissues encountered many experimental and analytic hurdles. Our work provides an alternative to existing methods to measure translation elongation speed through multiparametric flow cytometry data acquisition. The SunRiSE method is complementary to ribosomal profiling, since it provides quantitative information about translation activity in complex populations and at single-cell resolution, however, without giving information at the individual mRNA level. Importantly, it also permits a precise comparison of protein synthesis activity in cells from different origins. SunRiSE can also discriminate between cells displaying heterogeneous levels of actively progressing ribosomes from those with stalled ribosomes, which creates a high level of false-positive hits during ribosomal profiling (Zhang et al., 2017). This caveat highlights the need of techniques like SunRiSE that can overcome this limitation and can be used to evaluate the homogeneity of a cell population prior to analysis by ribosome profiling.

SunRiSE can be implemented with minimal laboratory equipment and is adapted to human clinical studies, since it requires only small numbers of cells isolated from blood or biopsies. Our observations suggest that eEF2 phosphorylation by eEF2K has the capacity to regulate both ribosome engagement and translation elongation, the latter being particularly obvious during ER stress induction. The heterogeneity of P-eEF2 levels in a given cell population, although it has no clear impact on translation, raises a question on the activation of eEF2K in culture conditions and whether only a subset of cells increases P-eEF2 in response to stress, and not the entire cell population, as previously assumed from bulk immunoblot-based studies (Boyce et al., 2008). In addition to being dependent on Ca^{2+}/calmodulin, eEF2K activity is negatively regulated by the mammalian target of rapamycin complex 1 (mTORC1). mTORC1, among other functions, controls both mRNA translation and ribosome biogenesis (Kenney et al., 2014). Importantly, the Cdc2–cyclin B complex has also been shown to regulate eEF2K in a cell cycle- and amino acid availability-dependent manner. Cdc2 is activated early in mitosis, targeting Ser359 in eEF2K and reducing eEF2 phosphorylation in mitotic cells (Smith and Proud, 2008). Inactivation of eEF2K by Cdc2 might keep eEF2 active during mitosis and permit protein synthesis to proceed, while explaining the heterogeneity observed among the single MEFs in culture. We could reveal that eEF2K controls the global level of ribosome engagement, something that was previously solely attributed to translation initiation factors. We cannot exclude that eEF2K inactivation impacts on mRNA transcription and stability, leading to an increase in the level of protein synthesis independently of translation initiation, but our results clearly underline the roles of eEF2 in controlling various steps of protein synthesis. Increased phosphorylation of eEF2 was thought to be the consequence of P-eIF2α accumulation in response to ER stress, with a direct role for eEF2K in translation inhibition (Boyce et al., 2008). Our results confirm that eEF2K is required to achieve efficient inhibition of protein synthesis during ER stress, potentially by impacting on translation initiation, through its interaction with the PERK/eIF2α pathway. Of course, one could foresee the existence of other eEF2K targets that could interfere with the initiation machinery, although recent characterization of such targets has not yielded any obvious alternative candidates other than eEF2 itself (Lazarus et al., 2017).

SunRiSE can be applied in different types of studies, whether they involve embryonic development, differentiation, activation, *ex vivo* characterization of cell subsets or cell cycle progression. Interestingly, different growth-promoting stimuli can have very different consequences on cell cycle entry and associated protein synthesis activity. Single-cell resolution offers a clear perspective on such different biochemical outcomes, and a combination of SunRiSE with techniques allowing the visualization of different cell cycle phases (Bajar et al., 2016) will be invaluable for our understanding of translation control during the cell cycle. In addition, to giving information on cell proliferation, the capacity of SunRiSE to be performed in bulk using biopsy samples, will also provide an original visualization of the immune cell metabolism in different pathogenic landscapes, such as tumor beds. Indeed, many cancers have the ability to produce factors (e.g. indoleamine 2,3-dioxygenase, or arginase I and II) able to inhibit protein synthesis in T cells and favor immune tolerance towards the tumors (Munn and Mellor, 2016). A technique like SunRiSE would now allow us to obtain a snapshot of tumor-associated immune cells with regard to their metabolic activity, with a prognostic value on their

Journal of Cell Science (2018) 131, jcs214346. doi:10.1242/jcs.214346

fitness and the tolerogenic impact of their immediate tumor environment. This technique could be further adapted to different physiological situations by using other inhibitors of the first translation elongation cycle, like lactimidomycin, which could be used as an alternative to harringtonine, to increase translation arrest efficiency in specific cell types or tissues, and thus further improve the accuracy of the method (Garreau de Loubresse et al., 2014). SunRiSE complements existing approaches to comparatively monitor protein synthesis, and its use in combination with previously existing techniques will assist in deciphering the complexity of the post-transcriptional regulation mechanisms that underlie the regulation of protein expression in most biological systems.

MATERIALS AND METHODS

Cell isolation and culture

WT and *eEF2K*$^{-/-}$ MEFs were obtained from Alexey Ryazanov (Rutgers University, Piscataway, NJ). MEFs and mouse splenocytes were cultured in Dulbecco's modified Eagle's medium (DMEM) containing 5% fetal calf serum (FCS) and 50 µM of 2-mercaptoethanol (MCCM; mouse cell culture medium) at 37°C under 5% CO_2. HeLa cells were cultured in DMEM with 10% FCS and 50 µM of 2-mercaptoethanol. To obtain splenocytes, 8-week-old wild type C57BL/6J mice were killed by cervical dislocation and splenectomized. Single-cells suspensions from the spleens were generated and cultured in MCCM. Cells were starved in Hank's balanced salt solution (HBSS) medium (Invitrogen, cat. no. 14185052) for 4 h, as previously described (Ingolia et al., 2012). Splenocytes were cultured in the absence (control) or presence of 0.1 µg/ml of lipopolysaccharide (LPS), or both PMA (5 ng/ml; Sigma, cat. no. P-8139) and ionomycin (500 ng/ml; Sigma, cat. no. I-0634) overnight. For ER stress induction, cells were treated with tunicamycin (100 ng/ml) for 16 h, thapsigargin for 3 h (500 nM), or with or without ISRIB (750 nM).

Labeling of protein nascent chains with puromycin

Cells from human blood, cell lines from *in vitro* culture or *ex vivo* mouse cells, were divided into 24-well plates (Fig. 1). Each well sample was treated with 2 µg/ml of harringtonine (Abcam, cat. ab141941), and after different time points, treated with puro (Sigma, cat. P7255) at 10 µg/ml (16.7 µM) (i.e. every 30 s for 7 min). Similar results were obtained by treating cells with harringtonine at different time points and adding puro (final concentration of 10 µg/ml) at the same time in all wells. After puro treatment, cells were washed in cold PBS and either stained (i.e. mouse splenocytes and fetal liver cells) with a combination of fluorophore-conjugated antibodies (see flow cytometry section) or directly fixed and permeabilized with BD Cytofix/Cytoperm™ (cat. no. 554714) followed by intracellular staining of puro using fluorescently labeled anti-puro antibodies for 1 h (1:1000, Clone 12D10, Merck, cat. no. MABE343).

Polysomal profiling by means of sucrose gradient fractionation

Polysomal mRNA molecules were enriched by sucrose gradient fractionation following the original protocol (del Prete et al., 2007). Briefly, 5×10^6 MEFs were lysed in 1 ml of polysome buffer [10 mM Tris-HCl pH 8, 140 mM NaCl, 1.5 mM $MgCl_2$, 0.5% NP40, 0.1 mg/ml cycloheximide, and 500 units/ml RNasin (Promega, Madison, WI)]. After 10 min on ice, lysates were quickly centrifuged (10,000 ***g*** for 10 s at 4°C) and the supernatant was resuspended in a stabilizing solution (0.2 mg/ml cycloheximide, 0.7 mg/ml heparin, 1 mM phenylmethanesulfonyl fluoride). After a quick centrifugation (12,000 ***g*** for 2 min at 4°C) to remove mitochondria and membrane debris, the resulting supernatant was layered on a 15% to 40% sucrose gradient. Gradients were then ultracentrifugated (35,000 ***g*** for 2 h at 4°C, SW41 rotor) and, after centrifugation, 20 fractions of 550 ml were collected, starting from the top of the gradient. All the fractions were then digested with proteinase K (200 mg/ml) in the presence of 1% SDS and 10 mM EDTA. RNA was then extracted with phenol/chloroform/isoamylalcohol (volume ratio 25:24:1) and precipitated with 2.5 volumes of 100% ethanol in the presence of 0.8 M lithium chloride. After precipitation, RNA was resuspended in RNase-free water. The correct fractionation of the polysomes was tested by measuring the ratio of different rRNA types on 1% denaturing agarose gel.

Immunoblotting

20 µg of NP-40 soluble material was separated by 4–12% gradient SDS-PAGE prior to immunoblotting and chemiluminescence detection (Pierce™). After performing SunRiSE on MEFs, puromycinilated peptide staining on immunoblots was performed using the monoclonal anti-puro antibody (1:5000; clone 12D10). Rabbit polyclonal antibodies anti-P-eEF2 and anti-eEF2 antibodies (Cell Signaling, cat. nos 2331 and 2332, both at 1:1000) were also used.

Flow cytometry

Cell suspensions were incubated with the antibody cocktail diluted in cold FACS buffer (PBS, 2% FCS, 2 mM EDTA) for 30 min at 4°C. Cells were fixed and permeabilized with cytofix/cytoperm buffer (BD Biosciences™), following the manufacturer's instructions, and stained for 1 h at 4°C with Alexa Fluor 488-conjugated anti-puro (puro-AF488) in PermWash. Flow cytometry was conducted by using BD LSR II and BD LSR Fortessa X-20 machines (BD Biosciences™), and data were analyzed with FlowJo (Tree Star™ or Cytobank). The antibodies used to stain cells were: puro-AF488 (1:100, Merck, cat. no. MABE343), phospho-S6-PE (1:600, Cell Signaling Technology, cat. no. #5316), Ki67 PE-eFluor 610 (1:400, eBioscience™, cat. no. 61-5698-82), anti-CD4-APC-eF780 (1:400, eBioscience™, cat. no. 47-0042-82), CD8-APC (1:600, eBioscience™, cat. no. 17-0081-83), CD80-PercPCy5.5 (1:600, Biolegend™, cat. no. 104722), anti-B220-BV421 (1:400, Biolegend™, cat. no. 103251), MHC-II-AF700 (1:800, eBioscience™, cat. no. 56-5321-82), and LIVE/DEAD™ Fixable Aqua Dead Cell Stain (Invitrogen™, cat. no. L34957). For proliferation assays, freshly isolated splenocyte suspensions were stained with CFSE. Briefly 1×10^7 cells per ml were incubated for 20 min with CellTrace Violet in 1× PBS following the manufacturer's instructions (Thermofisher Scientific, cat. no. 34557). Afterwards, the 1×10^7 splenocytes were treated with LPS or PMA/ionomycin or not (control), as mentioned above. After 48 h, SunRiSE was performed separately, and cells were stained with antibodies against CD4, CD3, CD19, MHC-II, CD11c, puro and Ki67.

Animal studies

Wild-type C57BL/6 mice were purchased from Charles River and maintained in the animal facility of CIML under specific pathogen-free conditions. C57Bl/6 embryos at E12.5 were depleted of all organs and brain, and dissociated in Liberase (0.5 mg/ml, Roche) and DNaseI (0.2 mg/ml, Roche) in PBS for 15 min at 37°C while stirring constantly. Cell suspensions were washed with RPMI (Thermo Scientific), supplemented with 2% heat-inactivated FCS, 100 U/ml penicillin and 100 mg/ml streptomycin prior to immunostaining and flow cytometry analysis. This study was carried out in strict accordance with the recommendations in the Guide for the Care and Use of Laboratory Animals, the French Ministry of Agriculture and of the European Union. Animals were housed in the CIML animal facilities accredited by the French Ministry of Agriculture to perform experiments on live mice. All animal experiments were approved by Direction Départementale des Services Vétérinaires des Bouches du Rhône (Approval number A13-543). All efforts were made to minimize animal suffering.

Statistical analysis

Statistical analysis was performed with GraphPad Prism software. For comparison of several conditions, we performed a one-way ANOVA, followed by a Tukey range test to assess the significance among pairs of conditions. When only two conditions were compared, we performed a Student's *t*-test or Welch *t*-test, according the validity of the homoscedasticity hypothesis. *P<0.05, **P<0.01, ***P<0.005.

Acknowledgements

We thank all CIML cytometry and Imaging core facilities for expert assistance and Dr A. Ryazanov for his kind gift of reagents. We acknowledge financial support from

the Agence Nationale de la Recherche ANR (ANR-10-INBS-04-01) to the France Bio Imaging and the ImagImm CIML imaging core facility.

Competing interests
The authors declare no competing or financial interests.

Author contributions
Conceptualization: P.P., R.J.A., M.R.S., A.M., A.G.T., L.R.d.P., E.G.; Methodology: P.P., R.J.A., M.R.S., A.M., V.C., S.A.v.d.P.; Formal analysis: V.C.; Investigation: R.J.A., M.R.S., A.M., V.C., S.A.v.d.P.; Writing - original draft: R.J.A., P.P.; Writing - review & editing: P.P., R.J.A., M.R.S., A.M., A.G.T., L.R.d.P., S.A.v.d.P., E.G.; Supervision: P.P., E.G.; Project administration: P.P., E.G.; Funding acquisition: P.P., E.G.

Funding
We are supported by grants from L'Association de la Recherche contre le Cancer to E.G. and P.P., and the Fondation pour la Recherche Medicale (FRM) (DEQ20140329536). The project was also supported by grants from the Agence Nationale de la Recherche (ANR) (ANR-12-BSV2-0025-01, ANR-FCT 12-ISV3-0002-01, INFORM Labex ANR-11-LABEX-0054, DCBIOL Labex ANR-11-LABEX-0043 and ANR-10-IDEX-0001-02; and PSL* and A*MIDEX projects ANR-11-IDEX-0001-02 funded by the 'Investissements d'Avenir' French government program). The research was also supported by the Ilídio Pinho Foundation and Fundação para a Ciência e a Tecnologia through the Institute for Biomedicine (iBiMED contract UID/BIM/04501/2013 and PTDC/IMI-IMU/3615/2014).

Supplementary information
Supplementary information available online at
http://jcs.biologists.org/lookup/doi/10.1242/jcs.214346.supplemental

References
Arava, Y., Wang, Y., Storey, J. D., Liu, C. L., Brown, P. O. and Herschlag, D. (2003). Genome-wide analysis of mRNA translation profiles in Saccharomyces cerevisiae. *Proc. Natl. Acad. Sci. USA* **100**, 3889-3894.

Azzam, M. E. and Algranati, I. D. (1973). Mechanism of puromycin action: fate of ribosomes after release of nascent protein chains from polysomes. *Proc. Natl. Acad. Sci. USA* **70**, 3866-3869.

Bajar, B. T., Lam, A. J., Badiee, R. K., Oh, Y.-H., Chu, J., Zhou, X. X., Kim, N., Kim, B. B., Chung, M., Yablonovitch, A. L. et al. (2016). Fluorescent indicators for simultaneous reporting of all four cell cycle phases. *Nat. Methods* **13**, 993-996.

Boyce, M., Py, B. F., Ryazanov, A. G., Minden, J. S., Long, K., Ma, D. and Yuan, J. (2008). A pharmacoproteomic approach implicates eukaryotic elongation factor 2 kinase in ER stress-induced cell death. *Cell Death Differ.* **15**, 589-599.

Brar, G. A. and Weissman, J. S. (2015). Ribosome profiling reveals the what, when, where and how of protein synthesis. *Nat. Rev. Mol. Cell Biol.* **16**, 651-664.

Buhr, F., Jha, S., Thommen, M., Mittelstaet, J., Kutz, F., Schwalbe, H., Rodnina, M. V. and Komar, A. A. (2016). Synonymous codons direct cotranslational folding toward different protein conformations. *Mol. Cell* **61**, 341-351.

David, A., Bennink, J. R. and Yewdell, J. W. (2013). Emetine optimally facilitates nascent chain puromycylation and potentiates the ribopuromycylation method (RPM) applied to inert cells. *Histochem. Cell Biol.* **139**, 501-504.

De Gassart, A. and Martinon, F. (2017). Translating the anticancer properties of eEF2K. *Cell Cycle* **16**, 299-300.

del Prete, M. J., Vernal, R., Dolznig, H., Mullner, E. W. and Garcia-Sanz, J. A. (2007). Isolation of polysome-bound mRNA from solid tissues amenable for RT-PCR and profiling experiments. *RNA* **13**, 414-421.

Dieterich, D. C., Hodas, J. J. L., Gouzer, G., Shadrin, I. Y., Ngo, J. T., Triller, A., Tirrell, D. A. and Schuman, E. M. (2010). In situ visualization and dynamics of newly synthesized proteins in rat hippocampal neurons. *Nat. Neurosci.* **13**, 897-905.

Garreau de Loubresse, N., Prokhorova, I., Holtkamp, W., Rodnina, M. V., Yusupova, G. and Yusupov, M. (2014). Structural basis for the inhibition of the eukaryotic ribosome. *Nature* **513**, 517-522.

Goodman, C. A., Pierre, P. and Hornberger, T. A. (2012). Imaging of protein synthesis with puromycin. *Proc. Natl. Acad. Sci. USA* **109**, E989.

Halstead, J. M., Lionnet, T., Wilbertz, J. H., Wippich, F., Ephrussi, A., Singer, R. H. and Chao, J. A. (2015). Translation. An RNA biosensor for imaging the first round of translation from single cells to living animals. *Science* **347**, 1367-1671.

Herbert, T. P. and Proud, C. G. (2006). Regulation of translation elongation and the cotranslational protein targeting pathway. In *Translational Control in Biology and Medicine*, (eds M. B. Mathews, N. Sonenberg, J. W. B. Hershey), pp 601-624. Cold Spring Harbor, NY: Cold Spring Harbor Laboratory Press

Ingolia, N. T., Ghaemmaghami, S., Newman, J. R. S. and Weissman, J. S. (2009). Genome-wide analysis in vivo of translation with nucleotide resolution using ribosome profiling. *Science* **324**, 218-223.

Ingolia, N. T., Brar, G. A., Rouskin, S., McGeachy, A. M. and Weissman, J. S. (2012). The ribosome profiling strategy for monitoring translation in vivo by deep sequencing of ribosome-protected mRNA fragments. *Nat. Protoc.* **7**, 1534-1550.

Kenney, J. W., Moore, C. E., Wang, X. and Proud, C. G. (2014). Eukaryotic elongation factor 2 kinase, an unusual enzyme with multiple roles. *Adv. Biol. Regul.* **55**, 15-27.

Lazarus, M. B., Levin, R. S. and Shokat, K. M. (2017). Discovery of new substrates of the elongation factor-2 kinase suggests a broader role in the cellular nutrient response. *Cell. Signal.* **29**, 78-83.

Lelouard, H., Schmidt, E. K., Camosseto, V., Clavarino, G., Ceppi, M., Hsu, H.-T. and Pierre, P. (2007). Regulation of translation is required for dendritic cell function and survival during activation. *J. Cell Biol.* **179**, 1427-1439.

McGlincy, N. J. and Ingolia, N. T. (2017). Transcriptome-wide measurement of translation by ribosome profiling. *Methods* **126**, 112-129.

Moore, C. E. J., Mikolajek, H., Regufe da Mota, S., Wang, X., Kenney, J. W., Werner, J. M. and Proud, C. G. (2015). Elongation factor 2 kinase is regulated by proline hydroxylation and protects cells during hypoxia. *Mol. Cell. Biol.* **35**, 1788-1804.

Munn, D. H. and Mellor, A. L. (2016). IDO in the tumor microenvironment: inflammation, counter-regulation, and tolerance. *Trends Immunol.* **37**, 193-207.

Petersen, C. P., Bordeleau, M.-E., Pelletier, J. and Sharp, P. A. (2006). Short RNAs repress translation after initiation in mammalian cells. *Mol. Cell* **21**, 533-542.

Richter, J. D. and Coller, J. (2015). Pausing on polyribosomes: make way for elongation in translational control. *Cell* **163**, 292-300.

Ryazanov, A. G. (2002). Elongation factor-2 kinase and its newly discovered relatives. *FEBS Lett.* **514**, 26-29.

Schmidt, E. K., Clavarino, G., Ceppi, M. and Pierre, P. (2009). SUnSET, a nonradioactive method to monitor protein synthesis. *Nat. Methods* **6**, 275-277.

Seedhom, M. O., Hickman, H. D., Wei, J., David, A. and Yewdell, J. W. (2016). Protein translation activity: a new measure of host immune cell activation. *J. Immunol.* **197**, 1498-1506.

Sekine, Y., Zyryanova, A., Crespillo-Casado, A., Fischer, P. M., Harding, H. P. and Ron, D. (2015). Stress responses. Mutations in a translation initiation factor identify the target of a memory-enhancing compound. *Science* **348**, 1027-1030.

Sidrauski, C., McGeachy, A. M., Ingolia, N. T. and Walter, P. (2015). The small molecule ISRIB reverses the effects of eIF2alpha phosphorylation on translation and stress granule assembly. *eLife* **4**, e05033.

Smith, E. M. and Proud, C. G. (2008). cdc2-cyclin B regulates eEF2 kinase activity in a cell cycle- and amino acid-dependent manner. *EMBO J.* **27**, 1005-1016.

Starck, S. R., Green, H. M., Alberola-Ila, J. and Roberts, R. W. (2004). A general approach to detect protein expression in vivo using fluorescent puromycin conjugates. *Chem. Biol.* **11**, 999-1008.

Tanenbaum, M. E., Stern-Ginossar, N., Weissman, J. S. and Vale, R. D. (2015). Regulation of mRNA translation during mitosis. *Elife* **4**, e07957.

tom Dieck, S., Kochen, L., Hanus, C., Heumüller, M., Bartnik, I., Nassim-Assir, B., Merk, K., Mosler, T., Garg, S., Bunse, S. et al. (2015). Direct visualization of newly synthesized target proteins in situ. *Nat. Methods* **12**, 411-414.

Wang, C., Han, B., Zhou, R. and Zhuang, X. (2016). Real-time imaging of translation on single mRNA transcripts in live cells. *Cell* **165**, 990-1001.

van de Pavert, S. A. and Vivier, E. (2016). Differentiation and function of group 3 innate lymphoid cells, from embryo to adult. Int Immunol. *Cell* **28**, 35-42.

Yan, X., Hoek, T. A., Vale, R. D. and Tanenbaum, M. E. (2016). Dynamics of translation of single mRNA molecules in vivo. *Cell* **165**, 976-989.

Yu, C. C.-W., Woods, A. L. and Levison, D. A. (1992). The assessment of cellular proliferation by immunohistochemistry: a review of currently available methods and their applications. *Histochem. J.* **24**, 121-131.

Yu, C.-H., Dang, Y., Zhou, Z., Wu, C., Zhao, F., Sachs, M. S. and Liu, Y. (2015). Codon usage influences the local rate of translation elongation to regulate co-translational protein folding. *Mol. Cell* **59**, 744-754.

Zhang, S., Hu, H., Zhou, J., He, X., Jiang, T., Zeng, J. (2017). Analysis of Ribosome Stalling and Translation Elongation Dynamics by Deep Learning. *Cell Syst.* **5**. 212-220.

Zanin-Zhorov, A., Tal-Lapidot, G., Cahalon, L., Cohen-Sfady, M., Pevsner-Fischer, M., Lider, O. and Cohen, I. R. (2007). Cutting edge: T cells respond to lipopolysaccharide innately via TLR4 signaling. *J. Immunol.* **179**, 41-44.

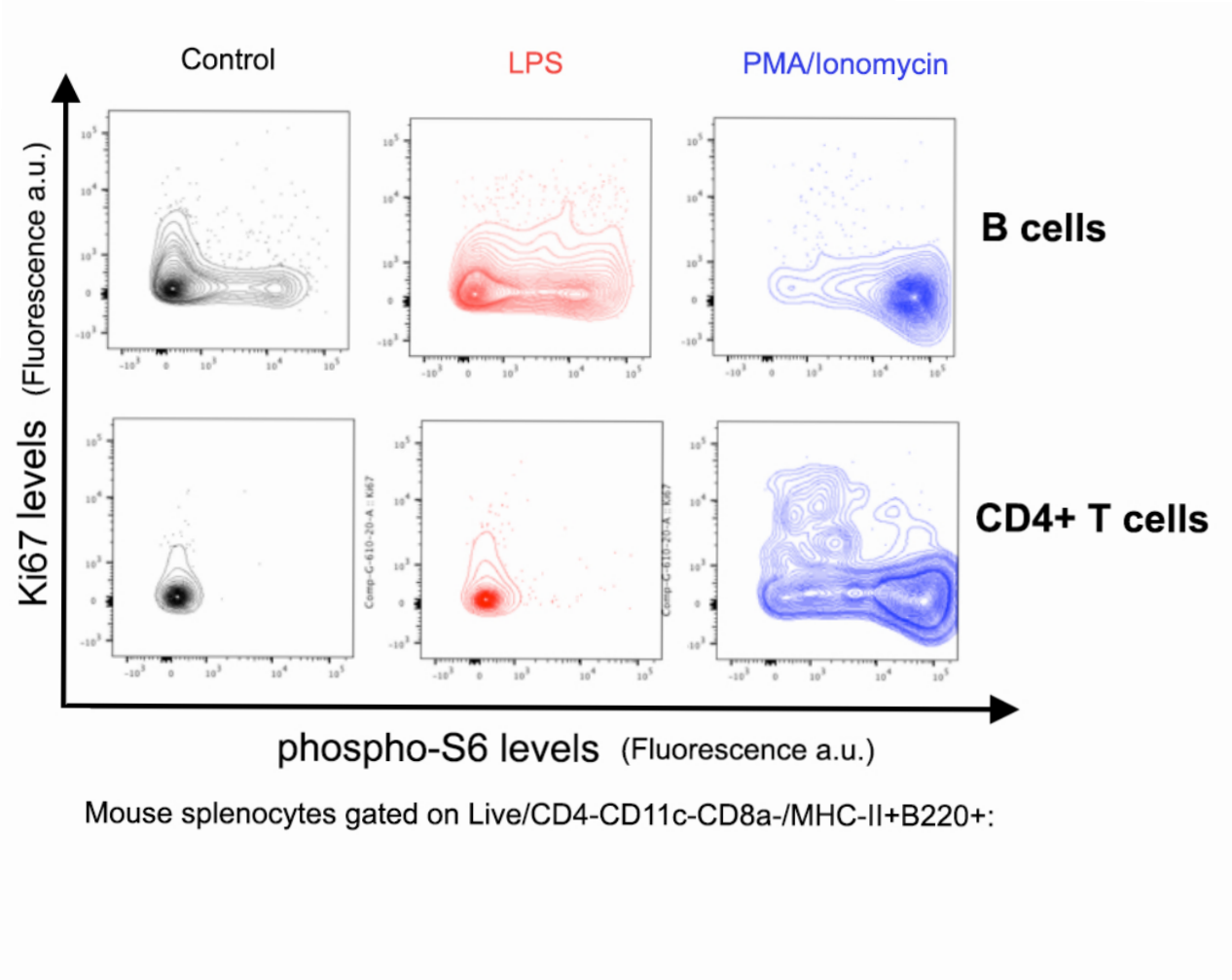

Figure S1. Phosphorylation of Ribosomal S6 protein in splenocytes after different stimuli. Mouse splenocytes were isolated and incubated for 16h with 10ng/ml of PMA and 1ng/ml of Ionomycin or LPS (100ng/ml) or non stimulated (Control). SunRiSE was performed together with CD4, CD8, CD19, CD11c, MHC-II and B220 flow cytometry staining to identify B and T Cells, as well as Ki67 and ribosomal P-S6 to evaluate entry in cell cycle and S6K1/2-mTORC1 activation. A) Dot plots showing P-S6 and Ki67 staining in CD4 T cells and B cells after different stimuli. The results are representative of one experiment (n=3, in duplicates).

Journal of Cell Science • Supplementary information

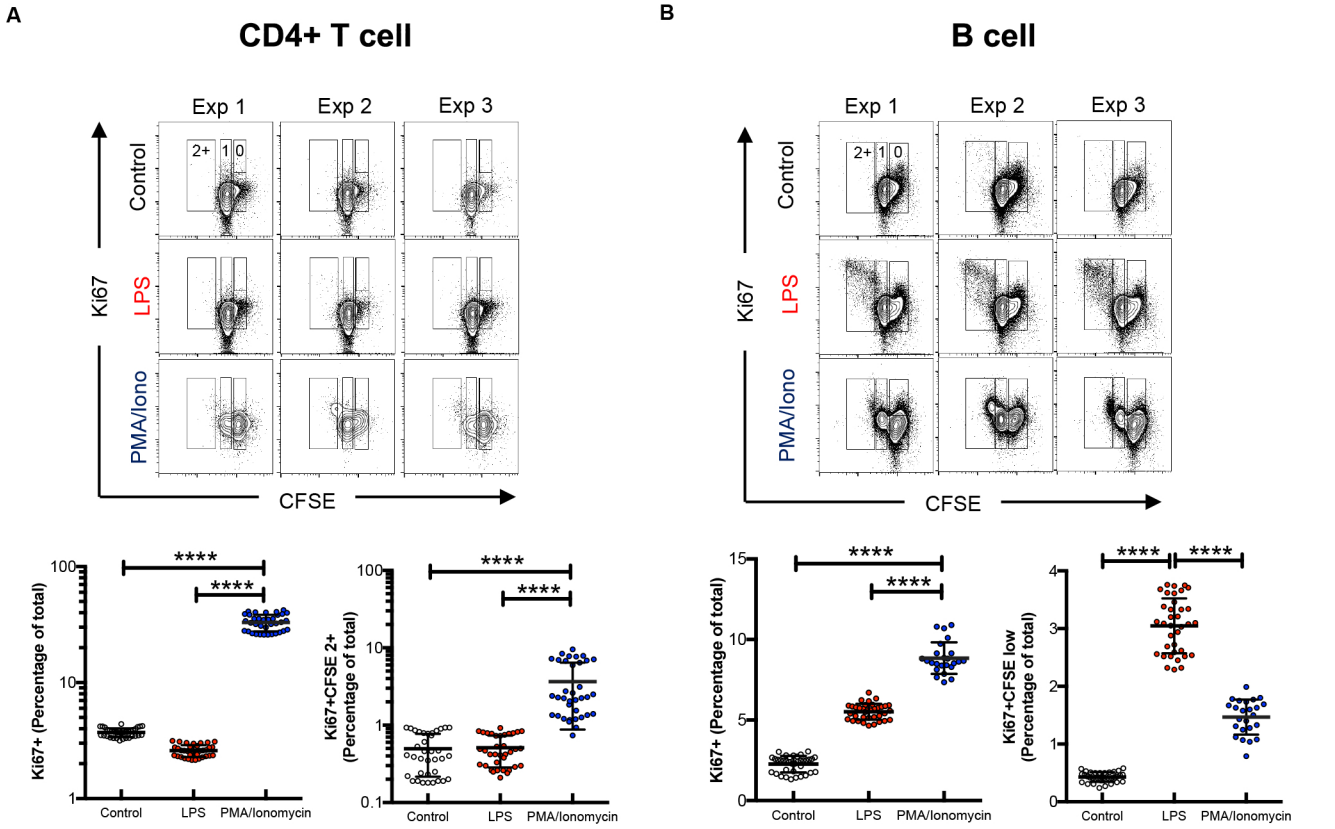

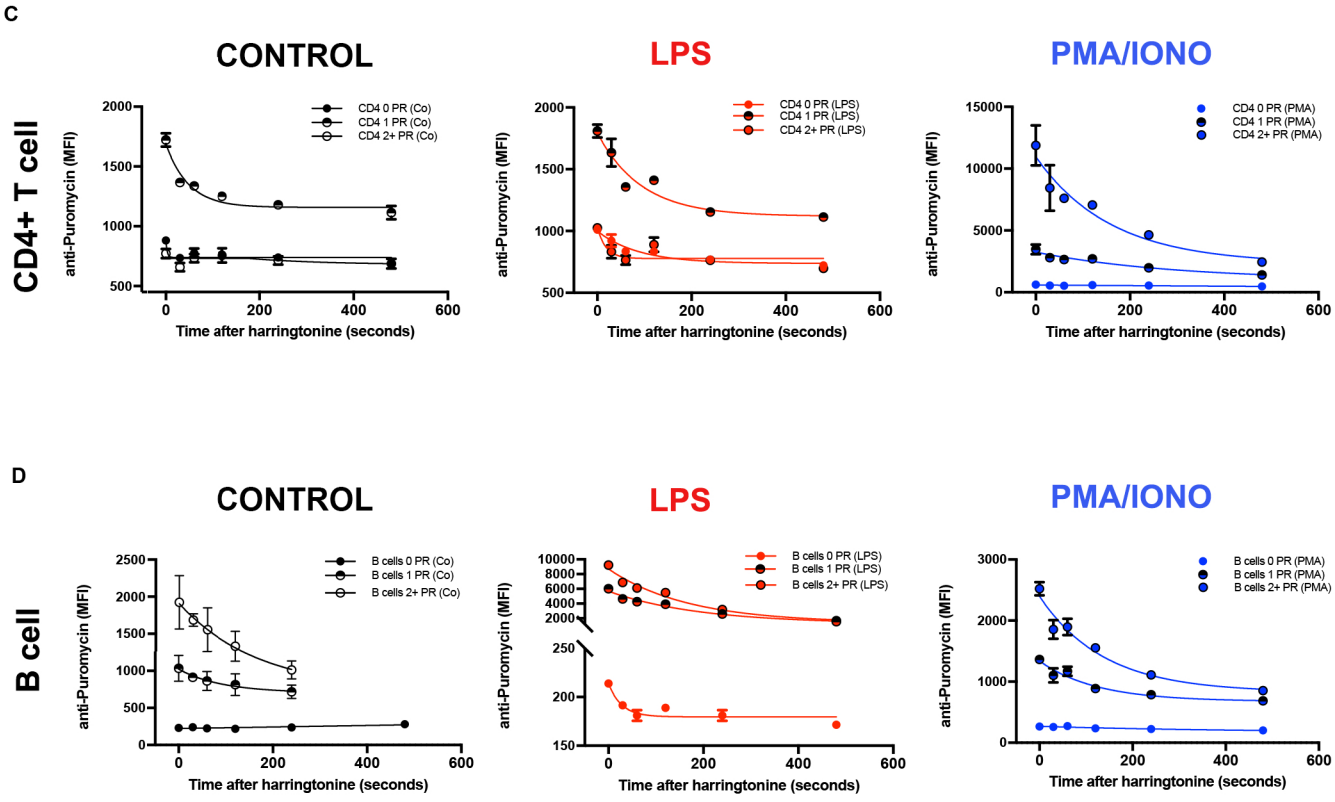

Journal of Cell Science • Supplementary information

Figure S2. Evaluation of proliferation, cell cycle marker and protein elongation in mouse splenocytes by SunRiSE. Mouse splenocytes were isolated and incubated for 48h with PMA/Ionomycin, LPS or non stimulated (Control). SunRiSE was performed together with CD3, CD4, CD8, CD19, CD11c, MHC-II and B220 flow cytometry staining to identify B and T Cells, as well as Ki67. A) Representative dot plots of CFSE dilution (gates on 0, 1 or 2 or more proliferation rounds, PR) in CD4+ T cells (upper panel) from different experiments (upper panel). Lower panel show quantification of the percentage of Ki67+ cells and the percentage of $CFSE^{low}Ki67^{+}$. B) Representative dot plots of CFSE dilution in B cells (upper panel) from different experiments (upper panel). Lower panel show quantification of the percentage of Ki67+ cells and the percentage of $CFSE^{low}Ki67^{+}$. C) Kinetics of SunRiSE in control and activated CD4 T cells in cells with different amount of proliferation rounds (PR) 0, 1 or 2 and more (2+). D) Kinetics of SunRiSE in control and activated B cells, gating on cells with different amount of proliferation rounds (PR) 0, 1 or 2 and more (2+). Mean ± SE levels of puro MFI (6 timepoints in duplicate) are plotted and datasets subjected to non-linear regression. The results are representative of one experiment (n=3, in duplicates). Statistical significance (*, $P<0.05$) was assigned usign PRISM software after comparing K values, 95% CI in Control vs LPS or PMA/Iono treated cells.

Journal of Cell Science • Supplementary information

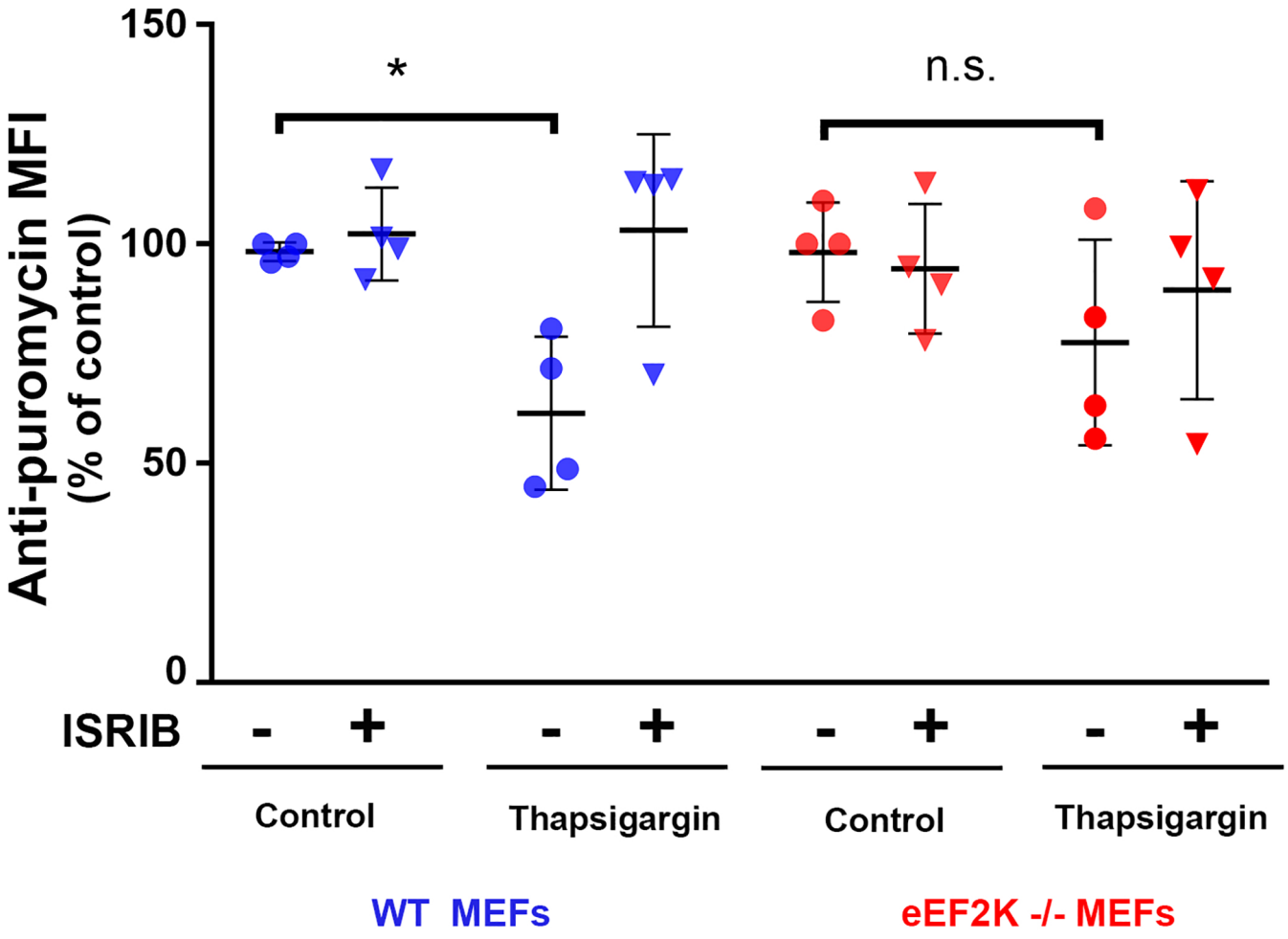

Figure S3. *eEF2K*$^{-/-}$ MEFs are resistant to thapsigargin accute stress. WT and *eEF2K*$^{-/-}$ MEFs were incubated with thapsigargin and ISRIB for 3h hours, prior to puro treament. After, the cells were fixed, permeabilized and stained with AF488-conjugated anti-puro antibody. After flow cytometry, mean fluorescence levels of anti-Puromycin were normalized to the MEF cells line control (t test, * P<0.05).

Journal of Cell Science • Supplementary information

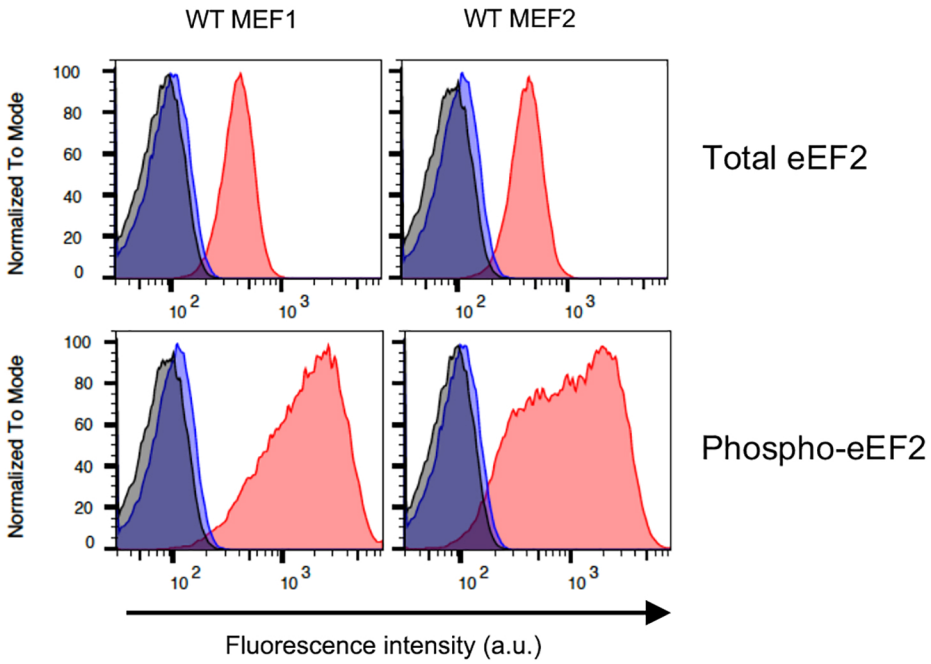

	TUBE NAME	Geometric Mean : Comp-G-PE-A
■	No Primary	74,4
■	Pre-Immune	91,9
■	anti-P-eEF2	1500

	TUBE NAME	Geometric Mean : Comp-G-PE-A
■	No Primary	73,2
■	Pre-Immune	85,8
■	anti-P-eEF2	901

	TUBE NAME	Geometric Mean : Comp-G-PE-A
■	No Primary	73,2
■	Pre-Immune	85,8
■	Total EEF2	399

	TUBE NAME	Geometric Mean : Comp-G-PE-A
■	No Primary	74,4
■	Pre-Immune	91,9
■	Total EEF2	419

Figure S4. Levels of total and phosphorylated EEF2 in MEFs. Different WT MEFs were incubated with either isotype control, polyclonal anti-total EEF2, or monoclonal anti-P-EEF2. While cells display homogeneous levels of total EEF2, while levels of P-EEF2 are heterogeneous.

Journal of Cell Science • Supplementary information